Spatial Distribution of Very Low Frequency and Low-Frequency (VLF/LF) Transmitter Signal Amplitude Associated With Lower Ionospheric Perturbations: Numerical Modeling and Observations

Yasuhide Hobara, Masahiko Iwamoto, and Masashi Hayakawa

Abstract – In this article, we conducted the numerical simulation of the subionospheric very low frequency (VLF) transmitter (TX) signals in the Earth–ionosphere waveguide using a two-dimensional finite-difference time domain method to study how the observed VLF amplitude varies with various perturbation conditions. As the simplest case, we assume a localized (Gaussian) ionospheric perturbation and calculate the relative change of the VLF TX electric amplitude on the ground in comparison to the quiet nighttime condition (without perturbation), as functions of horizontal perturbation scale, perturbation location, height, and distance from the TX. As a result, we found that the received TX amplitude greatly depends on the distance between the TX and ionospheric perturbation and on the spatial scale of the perturbations. We also demonstrate the comparison between the observed VLF TX electric amplitude and that of numerical computation to determine the perturbation properties of pre-earthquake ionospheric anomaly.

1. Introduction

Monitoring the very low frequency (VLF) transmitter (TX) signal is a very effective tool for detecting the lower ionospheric perturbations due to various geophysical phenomena occurring above and below it. For example, energetic particle precipitation from the magnetosphere [1], geomagnetic storms [2], solar flares [3], solar eclipse events [4], and gamma-ray bursts [5] occur above the ionosphere, while transient luminous events [6], intensive convection phenomena, such as thunderstorms and tropical cyclones [7], are atmospheric in origin. Perturbations due to the lithospheric origin before major earthquakes (EQs) have been reported [8–10]. However, the physical properties of seismoionospheric perturbation, such as spatial scale, density enhancement, and relative location from the epicenter, have not been well understood.

The received VLF TX wave amplitude generally changes in time when the lower ionosphere is disturbed around the path between a TX and receiver (RX). However, it is a difficult task, in general, to determine the location of the perturbation because the TX and RX are not in the same locations, like a bistatic radar, and because of the interference of VLF waves between different propagation modes in the Earth–ionosphere waveguide, especially at night.

Therefore, a detailed investigation of received TX amplitude dependence on the perturbation properties is extremely important for characterizing (identifying) the perturbation preceding the EQ and other perturbations caused by various factors. In particular, it is important to have a bird's-eye view of the changes in the received amplitude according to the location of the perturbation at each receiving point to determine the location of the perturbation.

In this study, we derived the dependence of the nighttime VLF TX wave electric amplitude on the distance from the TX and the perturbation location using a realistic ionospheric model based on the two-dimensional finite-difference time domain (2D-FDTD) method, assuming a lower ionospheric anomaly preceding an EQ. In this case, the spatial scale of the perturbation is assumed to be larger than the TX wave wavelength. The obtained results are further studied to extract major dependencies of the ionospheric properties. We also attempt to characterize the lower ionospheric perturbation by comparing the observed VLF amplitude anomaly before the EQ with results from the numerical calculations.

2. Numerical Computation

In this study, we perform numerical calculations using the 2D-FDTD. In this method, Maxwell's equations are directly solved for the numerous small finite cells, and spatiotemporal dependences of the VLF TX waves in different frequencies are computed in the realistic Earth–ionosphere waveguide. As a result,

Manuscript received 31 December 2022.

Yasuhide Hobara is with the Graduate School of Informatics and Engineering, School of Informatics and Engineering, and the Center for Space Science and Radio Engineering, The University of Electro-Communications, 1-5-1 Chofugaoka, Chofu, Tokyo, 1828585 Japan; e-mail: hobara@ee.uec.ac.jp

Masahiko Iwamoto is with the Graduate School of Informatics and Engineering, School of Informatics and Engineering, The University of Electro-Communications1-5-1 Chofugaoka, Chofu, Tokyo, 1828585 Japan.

Masashi Hayakawa is with Hayakawa Institute of Seismo Electromagnetics Co., Ltd., University of Electro-Communications Alliance Center 521, 1-1-1 Kojima-Cho, Chofu, Tokyo 1820026, Japan; e-mail: hayakawa@hi-seismo-em.jp.

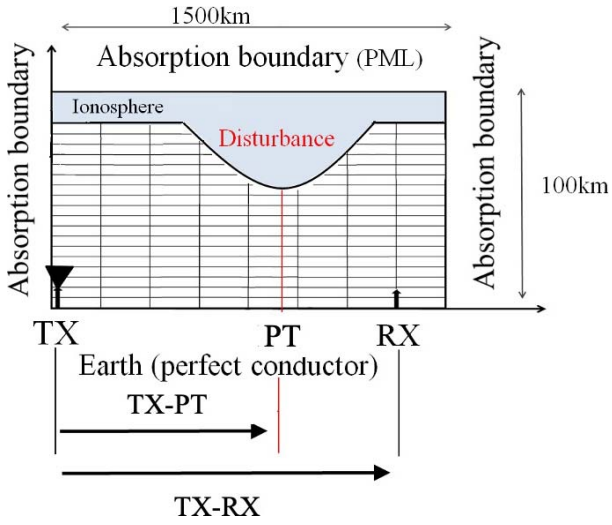

Figure 1. The geometry used for the numerical simulation of subionospheric VLF TX waves.

electric amplitude changes of the VLF signals are derived for the assumed ionospheric perturbation.

In Figure 1, the coordinate system of the numerical calculations is shown. We use a Cartesian coordinate system because of the relatively short VLF TX-RX distance (<1500 km). TX is located on the ground at the left-hand side edge of the horizontal axis (distance from the TX and RX). The vertical axis indicates the altitude from the ground. We assume the ground is a perfect conductor for simplicity, while the ionosphere is isotropic (Earth's magnetic field is not considered) for simplicity but has a finite conductivity with altitude dependence. The background nighttime electron density N_e and collision frequency ν with neutrals are taken from [11]. We apply the perfectly matched layer absorption boundary, except for the ground edge.

The ionospheric perturbations before the major seismic activities are assumed to be the local enhancement of the electron density directly over the epicenter characterized by the horizontal scale (W) of the Gaussian distribution, with a shift in the lower ionospheric height (H) at the perturbation center (PT; Figure 1). Because the spatial scale of the perturbations is assumed to be related to EQ parameters, such as the magnitude and depth, we examined combinations of two different horizontal scales ($W = 50$ km and 400 km) and two height shifts ($H = -1$ km and -4 km; i.e., four totally different cases). The negative sign of the shift in the ionospheric height indicates the ionospheric boundary decreases according to the previous reports of seismoionospheric anomaly [12, 13]. We assume the Japanese VLF TX (JJI, 22.2 kHz, Ebino, Miyazaki) and RX detecting the vertical electric amplitude at various locations from the TX.

3. Results and Discussion

In this section, we first present the general amplitude dependences of TX amplitude changes as functions of TX-RX distance and TX–ionospheric PT (over the epicenter; TX-PT) for several different special scales of the perturbations for rather short propagation distance (<1400 km), assuming the domestic TX (JJI). We demonstrate the distance variation of the simulated TX electric amplitude for one example of ionospheric perturbation associated with an EQ. The expected TX signal amplitude at a particular received station is compared with that of observation.

3.1 Amplitude Dependence on TX-RX Distance and Perturbation Location

Figures 2a–2d show examples of VLF TX amplitude changes as functions of TX-RX and TX-PT with four different combinations of horizontal scale (W) and ionospheric height change (H). From these figures, the amplitude changes are 1) mostly distributed in the forward scattered region (TX-PT < TX-RX) and 2) greatly vary with TX-RX, with a modal structure of both positive and negative values of amplitude change.

Concerning the amplitude change dependence on TX-RX, the longer the TX-RX distance, the longer the repetition period of its signature (positives and negatives). We only observe negative amplitude change over medium distances (TX-RX > 600 km and beyond). Interestingly, the sign of amplitude change remains the same, regardless of TX-PT for the same TX-RX. The amplitude change is largest when the PT is located in the middle of the TX-RX, and it becomes smaller when PT is located near the TX or RX.

As for the amplitude dependence on W in the TX-RX to TX-PT coordinate, patterns in the sign of amplitude remain the same, but the perturbed area slightly expands. On the contrary, the amplitude dependence on H is more pronounced both for short TX-RX (increase in amplitude change for 200 km to 400 km and ~0 dB) and long TX-RX (significant decrease in amplitude change beyond 600 km). Indeed, most previously reported seismoionospheric anomaly has a negative change in VLF amplitude (so-called *trend*; e.g., [9]) probably because of many of TX-RX > 500 km, so our numerical results well support these experimental results.

Although the previously mentioned complicated amplitude changes in the TX-RX – TX-PT coordinate are controlled by interferences from different propagation modes both from the unperturbed (background) and perturbed parts of the ionosphere in the Earth–ionosphere waveguide, we can suggest some practical approaches to detect and locate the seismoionospheric anomaly by distributing the observation sites to form the optimal VLF TX signal receiving network to be the most sensitive to the amplitude changes in TX-RX – TX-PT coordinate for the JJI TX. For example, at least one receiving station will be deployed in the longer distance TX-RX > 500 km, and a few more stations can be placed in the short distance range (TX-RX 200 km to 500 km). Amplitude changes in the TX-RX – TX-PT coordinate vary with TX frequency, so the same types

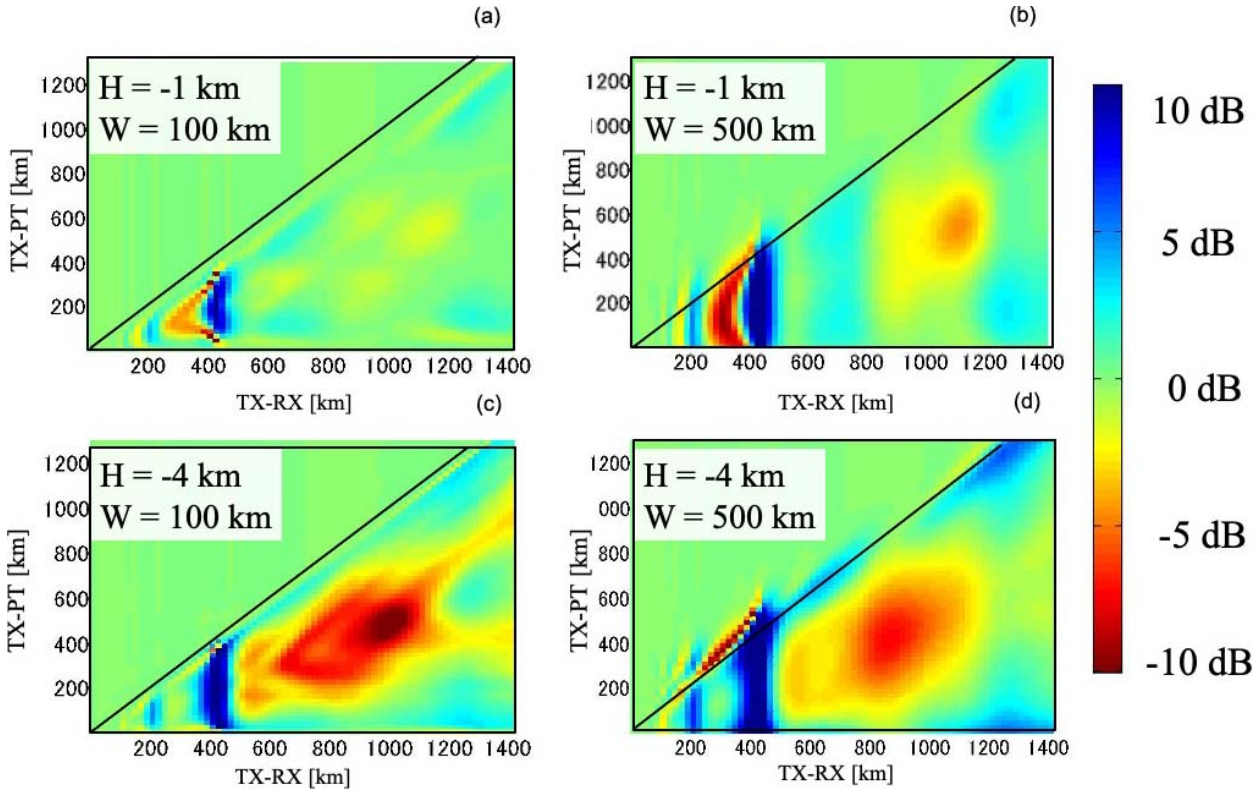

Figure 2. Spatial distributions of the VLF electric amplitude as functions of TX-RX distance and TX-PT (projection onto the ground) distance. Results from four different spatial conditions (a) to (d) horizontal scale (W) and vertical height change from the background (H) of perturbations.

of numerical calculations should be conducted to find out optical receiving locations for different TXs with different frequencies.

3.2 Application to Seismoionospheric Perturbation and Comparison With Observations

This section compares the modeled VLF TX amplitude with those from our observations. Vertical electric field intensity and phase changes of various VLF–low-frequency (VLF/LF) TXs are continuously recorded in the University of Electro-Communications VLF/LF observation network [2]. Our receiving station is equipped with a vertical electric field antenna, SoftPAL VLF RX unit, and the data logger. SoftPAL, version X, is a software radio RX that can provide temporal observations of the phase and amplitude of electromagnetic signals from multiple VLF TXs [14]. In this article, we used the vertical electric field data for our analysis. The temporal change of the electric amplitude of the TX signals contains information on the ionospheric perturbation around the TX-RX path. We use 2-min averaged amplitude time series data for seismoionospheric perturbations.

Figure 3a illustrates the locations of the Japanese VLF TX JJI and one of our VLF/LF receiving stations in Chofu, Tokyo (CHF), and the epicenter of the EQ analyzed in this study. EQ parameters were magnitude 6.2, occurred on August 1, 2011, at 14:58 UT, in the spatial coordinate (34.7°N, 1138.6°E), and with a depth ~23 km. We calculate the daily variations of the trend (averaged amplitude), dispersion (variability), and nighttime fluctuation [15] around the occurrence time of the EQ by using a local nighttime JJI TX amplitude time series.

Figures 3b–3c show the experimental data with the seismoionospheric anomaly for the EQ. Around 1 week before the EQ, a significant decrease in trend (top panel) and an increase in nighttime fluctuation are identified in the hatched region with a bin in Figure 3b. The diurnal amplitude pattern on the day of the anomaly is shown in Figure 3c, and the amount of decrease in amplitude in comparison to the averaged level for the last 30 d is –2.4 dB (median value for the nighttime period).

Figure 3d shows the calculated TX-RX dependences of the amplitude change for four different spatial scales of the ionospheric perturbations (combinations of the two horizontal scales, $W = 50$ km and 400 km, and two vertical height changes, $H = -1$ km and –4 km). The variation for $W = 400$ km and $H = -4$ km has the best agreement with the range of the observed amplitude change among four different sets of parameters. This perturbation size is within the EQ preparation zone by [16] (r (km) = 10^(0.43*EQ magnitude) ~463 km). Moreover, the derived vertical height change of –4 km is a reasonable value for seismoiono-

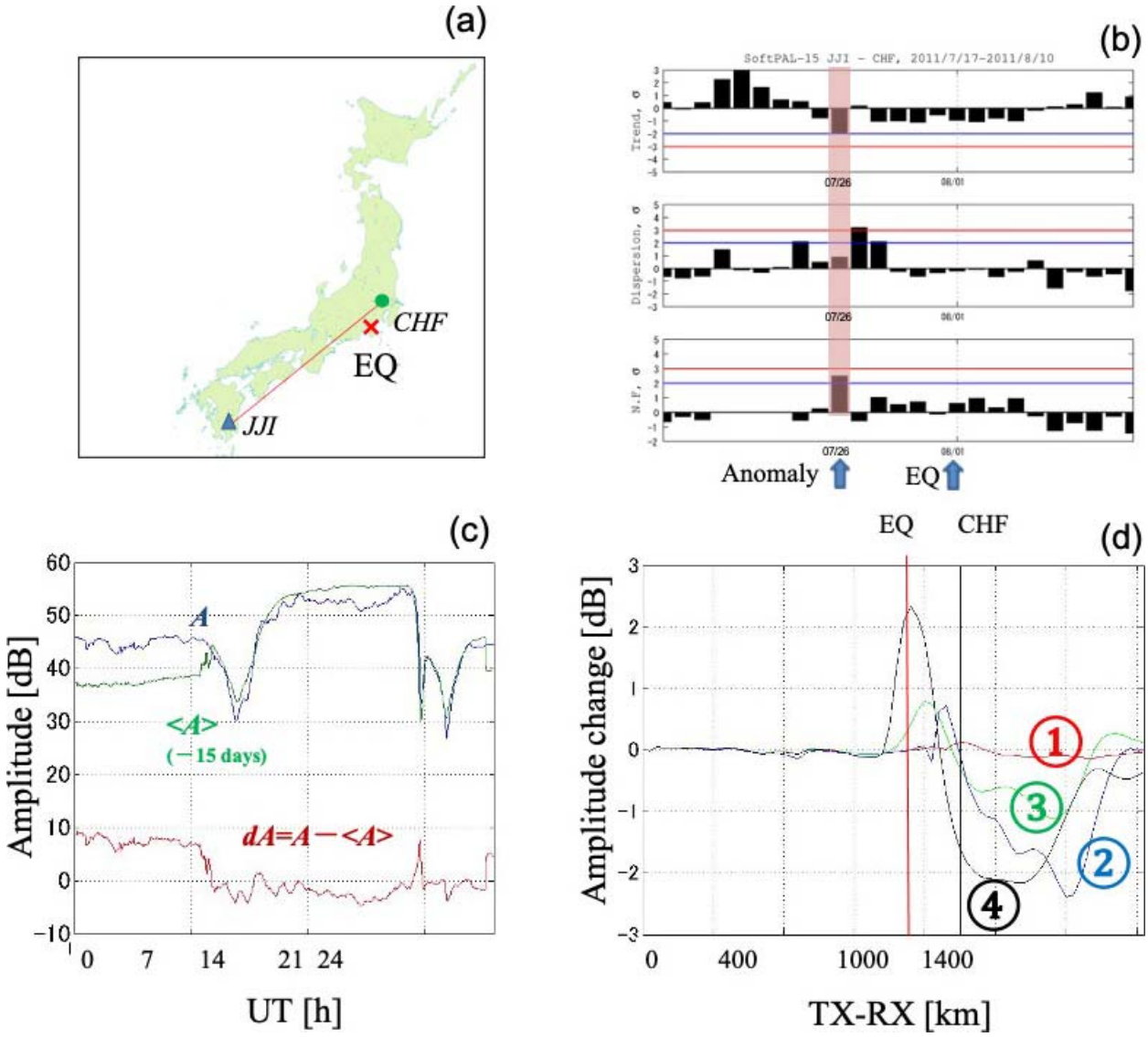

Figure 3. (a) Relative locations of the VLF TX (JJY) and receiving station (CHF) and the epicenter of the EQ. The propagation path between the JJI TX and the CHF RX is shown in the red line. (b) Comparison in VLF TX electric amplitude anomaly between observation and numerical model before EQ. Temporal evolution of three physical parameters (top, trend; middle, dispersion; bottom, nighttime fluctuation). (c) Diurnal variation for the anomaly day (July 26) before EQ, and the corresponding variation averaged over −15 d of the day (<A>) and residue (d$A = A -$ <A>), and (d) distance variation of electric amplitude change for four different perturbation conditions from the numerical simulations (1, $W = 50$ km, $H = -1$ km; 2, $W = 50$ km, $H = -4$ km; 3, $W = 400$ km, $H = -1$ km; 4, $W = 400$ km, $H = -4$ km).

spheric perturbation in comparison to the previous work using the wave hop method [12].

4. Conclusions

The spatial distributions of VLF TX electric amplitude with ionospheric perturbations are deduced using the 2D-FDTD method. Results from theoretical calculations indicate that the VLF RX amplitude change, including its signature, greatly varies with the TX distance from the RX, the location, and spatial extent (both horizontal and vertical) of the perturbations due to complex interference between different propagation modes, and perturbed subionospheric waves. In particular, the signature of perturbations varies rapidly with the short TX-RX distance, and the largest amplitude change is expected when the PT center is located around the midpoint of the TX-RX path.

Comparison in observed VLF TX amplitude anomaly due to the ionospheric perturbation before an EQ with those from numerical computations with various ionospheric conditions was made, and rather good agreement has been obtained for a particular set of perturbation parameters. Therefore, the combinations of numerical models and observation can be used to determine the perturbation properties.

The numerically obtained spatial distributions of VLF TX signals also provide useful information on suitable RX locations to deduce the possible location and spatial extent of the ionospheric perturbation by using combinations of TX-RX paths from the VLF TX signal receiving network. In the future, we will further develop our two-dimensional model to three dimensional with an anisotropy of the ionosphere, and we can examine the case in which the perturbation is dislocated from the TX-RX path with an arbitrary spatial shape of perturbations.

5. References

1. U. S. Inan, S. A. Cummer, and R. A. Marshall, "A Survey of ELF and VLF Research on Lightning-Ionosphere Interactions and Causative Discharges," *Journal of Geophysical Research*, **115**, A6, June 2010, doi: 10.1029/2009JA014775.
2. K. Tatsuta, Y. Hobara, S. Pal, and M. Balikhin, "Sub-Ionospheric VLF Signal Anomaly due to Geomagnetic Storms: A Statistical Study," *Annales Geophysicae*, **33**, 11, November 2015, pp. 1457-1467.
3. B. Singh, R. Tyagi, Y. Hobara, and M. Hayakawa, "X-Rays and Solar Proton Event Induced Changes in the First Mode Schumann Resonance Frequency Observed at a Low Latitude Station Agra, India," *Journal of Atmospheric and Solar-Terrestrial Physics*, **113**, June 2014, pp 1-9.
4. D. Inui and Y. Hobara, "Spatio-Temporal Characteristics of Sub-Ionospheric Perturbations Associated With Annular Solar Eclipse Over Japan: Network Observations and Modeling," 2014 XXXIth URSI General Assembly and Scientific Symposium, Beijing, China, August 16–23, 2014, doi: 10.1109/ URSIGASS.2014.6929555.
5. M. B. Cohen, U. S. Inan, and G. Fishman, "Terrestrial Gamma Ray Flashes Observed Aboard the Compton Gamma Ray Observatory/Burst and Transient Source Experiment and ELF/VLF Radio Atmospherics," *Journal of Geophysical Research*, **111**, D24, December 2006, doi: 10.1029/2005-JD006987.
6. Y. Hobara, N. Iwasaki, T. Hayashida, M. Hayakawa, K. Ohta, et al., "Interrelation Between ELF Transients and Ionospheric Disturbances in Association With Sprites and Elves," *Geophysical Research Letters*, **28**, 5, March 2001, pp. 935-938.
7. S. Pal, S. Sarkar, S. K. Midya, S. K. Mondal, and Y. Hobara, "Low Latitude VLF Radio Signal Disturbances due to the Extremely Severe Cyclone Fani of May 2019 and Associated Mesospheric Response," *Journal of Geophysical Research*, **125**, 5, May 2020, p. e2019JA027288.
8. V. Singh and Y. Hobara, "Simultaneous Study of VLF/ULF Anomalies Associated With Earthquakes in Japan," *Open Journal of Earthquake Research*, **9**, 2, March 2020, pp. 201-215.
9. M. Hayakawa and Y. Hobara, "Current Status of Seismo-Electromagnetics for Short-Term Earthquake Prediction," *Geomatics, Natural Hazards and Risk*, **1**, 2, June 2010, pp. 115-155.
10. S. Potirakis, T. Asano, and M. Hayakawa, "Criticality Analysis of the Lower Ionosphere Perturbations Prior to the 2016 Kumamoto (Japan) Earthquakes as Based on VLF Electromagnetic Wave Propagation Data Observed at Multiple Stations," *Entropy*, **20**, 3, March 2018, pp. 199-215.
11. J. R. Wait and K. P. Spies, *Characteristics of the Earth-Ionosphere Waveguide for VLF Radio Waves*, technical note 300, National Bureau of Standards, Boulder, CO, December 1964.
12. M. Yoshida, T. Yamauchi, T. Horie, and M. Hayakawa, "On the Generation Mechanism of Terminator Times in Subionospheric VLF/LF Propagation and Its Possible Application to Seismogenic Effects," *Natural Hazards and Earth System Sciences*, **8**, 1, February 2008, pp. 129-134.
13. M. Hayakawa, Y. Kasahara, T. Nakamura, F. Muto, T. Horie, et al., "A Statistical Study on the Correlation Between Lower Ionospheric Perturbations as Seen by Subionospheric VLF/LF Propagation and Earthquakes," *Journal of Geophysical Research*, **115**, A9, September 2010, doi: 10.1029/2009JA015143.
14. R. L. Dowden and C. D. D. Adams, "SoftPAL," 3rd VERSIM Workshop, Tihany, Hungary, September 15–20, 2008, pp. 15-20.
15. M. Hayakawa, Y. Hobara, H. Yamaguchi, K. Ohta, J. Izutsu, et al., "A Possible Precursor to the 2011 3.11 Japan Earthquake: Ionospheric Perturbations as Seen by Subionospheric VLF/LF Propagation," *Annals of Geophysics*, **55**, 1, April 2012, pp. 95-99.
16. I. P. Dobrovolsky, S. I. Zubkov, and V. L. Miachkin, "Estimation of the Size of Earthquake Preparation Zones," *Pure and Applied Geophysics*, **117**, September 1979, pp. 1025-1044.